

Influence of freeze–thaw cycles on the pull-out response of lime-based TRM composites

Dalalbashi, Ali; Ghiassi, Bahman; Oliveira, Daniel V.

DOI:

[10.1016/j.conbuildmat.2021.125473](https://doi.org/10.1016/j.conbuildmat.2021.125473)

License:

Creative Commons: Attribution-NonCommercial-NoDerivs (CC BY-NC-ND)

Document Version

Peer reviewed version

Citation for published version (Harvard):

Dalalbashi, A, Ghiassi, B & Oliveira, DV 2021, 'Influence of freeze–thaw cycles on the pull-out response of lime-based TRM composites', *Construction and Building Materials*, vol. 313, 125473.

<https://doi.org/10.1016/j.conbuildmat.2021.125473>

[Link to publication on Research at Birmingham portal](#)

General rights

Unless a licence is specified above, all rights (including copyright and moral rights) in this document are retained by the authors and/or the copyright holders. The express permission of the copyright holder must be obtained for any use of this material other than for purposes permitted by law.

- Users may freely distribute the URL that is used to identify this publication.
- Users may download and/or print one copy of the publication from the University of Birmingham research portal for the purpose of private study or non-commercial research.
- User may use extracts from the document in line with the concept of 'fair dealing' under the Copyright, Designs and Patents Act 1988 (?)
- Users may not further distribute the material nor use it for the purposes of commercial gain.

Where a licence is displayed above, please note the terms and conditions of the licence govern your use of this document.

When citing, please reference the published version.

Take down policy

While the University of Birmingham exercises care and attention in making items available there are rare occasions when an item has been uploaded in error or has been deemed to be commercially or otherwise sensitive.

If you believe that this is the case for this document, please contact UBIRA@lists.bham.ac.uk providing details and we will remove access to the work immediately and investigate.

Influence of freeze-thaw cycles on the pull-out response of lime-based TRM composites

Ali Dalalbashi¹, Bahman Ghiassi², Daniel V. Oliveira³

ABSTRACT

Textile reinforced mortars (TRMs) have emerged as a sustainable solution for strengthening existing masonry and concrete structures. As a result, many recent studies have focused on understanding the performance of these composites. However, most of these are aimed at investigating the mechanical properties of TRM composites. At the same time, their durability and long-term performance remain poorly addressed and unclear. This paper presents an experimental study on the effect of freeze-thaw environmental conditions on the micro-mechanical behavior of these composites. The results indicate that the freezing-thawing exposure conditions considered in this study do not have detrimental effects on the mortar strength. However, the fiber-to-mortar bond behavior can deteriorate because the deterioration level depends on the fiber type, embedded length, and fiber configuration.

Keywords: Fiber/matrix bond; Pull-out test; Durability; Freeze-Thaw; Hydraulic lime mortar; TRM; FRM; SRG

¹ PhD student, University of Minho, ISISE, Department of Civil Engineering, Guimarães, Portugal. E-mail: alidalalbashi@gmail.com. <https://orcid.org/0000-0003-0486-1433>

² Assistant Professor, University of Nottingham, Centre for Structural Engineering and Information, Faculty of Engineering, Nottingham, United Kingdom. E-mail: bahman.ghiassi@nottingham.ac.uk. <http://orcid.org/0000-0003-4212-8961>

³ Associate Professor, University of Minho, ISISE, Department of Civil Engineering, Azurém, 4800-058 Guimarães, Portugal. E-mail: danvco@civil.uminho.pt. <http://orcid.org/0000-0002-8547-3805>

1 Introduction

Textile reinforced mortar (TRM) has recently raised interest among researchers and professionals as a sustainable and compatible solution for strengthening existing structures. TRM composites, also referred to as FRCM and TRC in the literature, have clear advantages when compared to fiber-reinforced polymer sheets (FRPs), such as fire resistance, sustainable and durable alternative to epoxy [1–3]. TRM composites consist of cement or lime-based mortar reinforced by steel, glass, basalt, carbon, or natural fibers. Lime-based mortars are suitable for strengthening masonry and historic structures because of their physical, chemical, and mechanical compatibility with the substrate [4,5].

The effectiveness of TRM strengthening systems depends on the fiber-to-mortar and TRM-to-substrate bond performance and their mechanical behavior, which have been investigated in many recent studies [6–12]. Besides, a pseudo-ductile performance of TRM composites due to the multiple cracking leads these composites to be suitable for seismic strengthening. The fiber-to-mortar bond strength provides this multiple cracking behavior [13]. Therefore understanding this mechanism and its long-term performance under harsh environmental conditions is vital for having safe and resilient strengthening solutions.

The durability performance of TRM composites has recently received attention from a few studies. These studies mainly focused on the tensile response, flexural behavior, and TRM-to-substrate bond performance under high-temperature, salt crystallization, and alkaline environments [14–20]. Different fiber and mortar types were used to investigate the effect of freeze-thaw (FT) conditions on the mechanical behavior of TRM composites, regardless of the number of FT cycles applied to the specimens [21–26]. The FT conditions increased the ultimate tensile strength of carbon and PBO-based FRCM composites by 11-13% [24,25] and 32% [24], respectively. An earlier study [26] determined that glass-based FRCMs had a constant ultimate tensile strength after applying 40 FT cycles. Meanwhile, some studies report that TRM composites exhibit a reduction in mechanical properties. For instance, the tensile and flexural strength of glass-based TRC composites decreased by 16% to 19% [21,23] and 19% [22], respectively. As a result, freeze-thaw conditions affected the mechanical performance of TRM composites differently. Additionally, in these studies, the exposed specimens were compared with control specimens at zero cycles, which can lead to an error in the analysis (especially if the matrix is a lime-based mortar). However, these studies are limited in scope, and further investigations are needed to fully understand the governing

deterioration mechanisms and field performance of these composites. Also, investigations on the effect of environmental conditions on the micro-mechanical response of these composites are still lacking [27].

This study aims to investigate the role of freeze-thaw (FT) conditions on the micro-mechanical response of TRM composites. FT conditions are chosen as one of the critical environmental conditions, especially when TRMs are applied on the outside of the buildings. Two different TRM systems (glass-based and steel-based) commonly used to repair existing masonry structures are used for the purpose of this study. The tests include mechanical characterization of the mortar and the fibers, as well as bond tests to characterize the role of embedded length and fiber configuration on the fiber-to-mortar bond behavior.

2 Experimental program

The aim is to investigate experimentally the changes in material properties and fiber-to-mortar bond behavior under FT conditions. To this end, a set of TRM composite specimens (specimen details are presented in sections 2.1 to 2.3) was prepared. After 90 days of curing in the laboratory, the specimens were exposed to zero, 60, 180, 300, and 360 FT cycles described in section 2.4 or stored in the environmental lab condition as control specimens. After that, a series of post-exposure material properties and pull-out tests (on steel and glass-based TRM composites) were conducted (see Table 1 for a detailed experimental plan and the number of specimens).

The pull-out specimens (which were prepared based on fiber types, bond length, and fiber configuration) are named as VWX-YZ; where V is related to the fiber type (S: steel, G: glass), and W is linked to the fiber configuration (S: single cord/yarn, T: single yarn + transverse elements, G: two cords/yarns, G': four cords). In addition, X is connected to the different embedded lengths (for glass: 50, 75, and 100 mm, for steel: 50, 150, 200, and 250 mm). Finally, Y is related to the control (C) or exposed (E) specimens, and Z represents the number of FT cycles (0, 60, 180, 300, and 360). For example, GS50-E60 is a glass-based TRM composite with a single yarn and 50 mm bond length exposed to 60 FT cycles. The materials description, sample preparation, and test methods are presented in the following sections.

2.1 Materials

All specimens were prepared using a commercial mortar, which was a hydraulic lime (NHL) and eco-pozzolan-based mortar. The reinforcing materials were a unidirectional steel mesh and woven

biaxial glass fabric mesh. Each cord of the steel mesh was made by twisting five individual wires, with a density of 670 g/m² and an effective area of 0.538 mm². The alkali-resistance glass fabric had a mesh size and area per unit length equal to 25×25 mm² and 35.27 mm²/m, respectively. All specimens, including the material characterization and the pull-out tests, were cured under the same procedure until the test dates. Three days after the preparation of specimens, they were demolded. All specimens were cured under wet clothes and plastic for the first seven days, then stored and subjected to environmental lab conditions for 83 days. Earlier studies by the authors [12,27] have shown that the early maximum strength of the lime-based mortar occurs after 90 days. Then, one part of the specimens was exposed to the planned FT cycles, while the remaining specimens were kept in the lab as control specimens and tested simultaneously with the exposed specimens (see Fig. 1 and Table 1).

2.2 Materials characterization test

Differential thermal analyses (DTA) were conducted with a Q600 TA Instrument apparatus to quantify and identify chemical composition by observing the thermal behavior of mortar samples after different exposure times. The mortar samples were heated from 50°C to 1000°C at a rate of 10°C/min in an aluminum pan and under 100 ml/min of N₂ flow. All DTA samples (25 mg) were extracted from the pull-out specimens at the bond interface after testing (for each series, three samples were prepared).

The compressive strength of mortar was measured by performing cubic specimens (50×50×50 mm³) and following ASTM C109 [28]. The tests were performed under force-controlled conditions, at a rate of 10 N/s, and using a Lloyd testing machine, as shown in Fig. 2a. The flexural strength of the mortar was tested according to EN 1015-11 [29], where specimens had a prismatic shape (40×40×160 mm³). Three-point bending tests were conducted for this purpose with a Lloyd testing machine under force-controlled conditions at a rate of 150 N/s (Fig. 2b). Additionally, the elastic modulus of mortar was characterized according to EN 12390-13 [30] using cylinder-shaped specimens (150 mm in length and 70 mm diameter) and using a universal testing machine (load capacity of 100 kN). Three LVDTs with a 5 mm range and 1-μm sensitivity were mounted on the specimens to measure the deformations of specimens (see Fig. 2c).

The fabric tensile strength was characterized by performing direct tensile tests on the single steel cords and single glass yarns (warp direction). A universal testing machine (load capacity of 10 kN)

under displacement-controlled conditions (0.3 mm/min) applied tensile loads to the samples. A 100 mm clip gauge located at the center of the specimens was used to measure the deformations during the tests, as shown in Fig. 2d.

2.3 Pull-out tests

A single-sided pull-out test setup developed in [31] was used to investigate the fiber-to-mortar bond behavior. The samples were prepared following the methodology explained in [31] and the geometry shown in Fig. 3a. Preparation of pull-out specimens firstly involved embedding the fiber in an epoxy resin block in 200 mm length. The pull-out specimens had a flat disk-shaped mortar with a width of 125 mm and a thickness of 16 mm. Pull-out specimens were prepared by applying 8 mm of mortar to the inside of the wood mold, placing fibers, and then applying another layer of mortar with 8 mm thick. To evaluate the role of the fabric architecture, different configurations were considered for each type of fiber. In the steel-based TRM, which was composed of a unidirectional steel mesh, this consisted of evaluating the role of the cords number ("single cord," "two cords," and "four cords") and embedded length (50, 150, 200, and 250 mm), as presented in Fig. 3b. It should be mentioned that samples were prepared with only 150 mm embedded length. Since the glass fabric was a bidirectional mesh, the samples consisted of: "single (warp) yarn," "single yarn + transverse elements," and "group of yarns" (Fig. 3c). The bond length of the "single yarn" specimens was 50, 75, and 100 mm, while the bond length of other groups was 50 mm. The considered bond length for the steel and glass-based TRMs was determined based on the experimental results reported by the authors in [32]. In the "single yarn + transverse elements" specimens, two transverse elements (weft yarns) were embedded in the mortar with a total length of 25 mm, 12.5 mm at each side, equal to half of the mesh opening. In the "group of yarns," two weft yarns were embedded in the mortar, in which their total lengths were equal to 50 mm (12.5 mm at each side and 25 mm distance between warp yarns), as shown in Fig. 3c.

For performing the pull-out tests, two U-shape steel supports fixed the specimens (see Fig. 3d). A servo-hydraulic system (load capacity of 25 kN) applied tensile loads to the epoxy resin block from the top with a mechanical clamp under displacement-controlled conditions and at a rate of 1.0 mm/min. Three LVDTs with a 20 mm range and 2- μ m sensitivity measured the fiber-to-mortar slip. LVDT average measurements are shown as slip in the results of the experiment.

2.4 Environmental conditions

A Fitoclima 6400 EC25 climatic chamber was used to expose the samples to freeze-thaw (FT) conditions. The FT cycles consisted of thawing the samples at 30°C and 90% RH for two hours; then, the temperature was decreased at a 0.111°C/min rate until reaching -10°C. After this point, samples were frozen for two hours, followed by a temperature increase at a rate of 0.111°C/min till reaching 30°C. Fig. 4a shows the planned and the real conditions (including temperature and humidity) inside the climatic chamber, where the real temperature and humidity were measured by the average of two standalone data loggers.

This cycle of sixteen hours was repeated 360 times. The selected FT environmental condition aimed to create an environment in the laboratory to represent real environmental conditions in an accelerated way. A similar FT condition was also performed in another study [33] to investigate the performance of FRP strengthening systems. Several control samples were also prepared and placed in the laboratory in parallel to the FT tests. The environmental conditions of the storage laboratory during this period are presented in Fig. 4b (average temperature and humidity were 18°C and 75% RH).

Five specimens from each series of tests (material characterization and pull-out tests) were taken from the climatic chamber room (at 20°C) per 60 cycles (equal to 40 days), as presented in Fig. 1. They were then placed in the laboratory conditions for seven days before performing the post-exposure tests.

3 Results and discussion

3.1 Material properties

DTA analysis graph shows three peaks (Fig. 5) attributed to hydrated water (50-100°C), dehydroxylation (losing bound water at 380-400°C), and decarboxylation (releasing CO₂ at 680-780°C) [34–37]. DTA results show that decarboxylation increases with time under both the control and the FT conditions due to the large amount of CaCO₃ when it is compared to the control specimens at 90 days of age (C0). The dehydroxylation and decarboxylation changes obtained from the DTA test show that the used lime-based mortar is still hardening at older ages under both the control and the FT conditions. Generally, hydraulic lime-based mortar hardens with a combination of hydration and carbonation, according to [38]. Therefore, from these outputs and

previous results [27], it can be concluded that using a hydraulic lime-based mortar at an early age for durability tests can lead to erroneous results.

Table 2 reports the changes in the strength of mortar and fibers under both the control and the FT conditions. The mortar compressive strength remains constant until the end of tests under both conditions. However, by ignoring the variation of the results, the mortar compressive strength shows a slight increment. This increment is 3% in the control samples (C360), and 12% in the FT exposed samples (E360) when compared to the control specimens at zero cycles (C0). Similar behavior is also observed for the flexural strength and the elastic modulus. These observations show that the considered FT conditions do not have a detrimental effect on the mortar strength but lead to a slight enhancement of properties, possibly by promoting mortar hydration under high humidity conditions, which is in line with the DTA results. Besides, results are consistent with the changes in mortar strength under indoor conditions reported in [27]. As for the fibers, glass yarns do not show any deterioration, but the tensile strength of steel cords and elastic modulus under the FT conditions declined slightly by 5% and 9%, respectively.

3.2 Effect of embedded length on the pull-out response

3.2.1 *Steel-reinforced mortar*

Fig. 6 shows the average load-slip curves of steel-based TRM with different embedded lengths under both the control and the FT conditions. Table A 1 also presents the failure mode of these specimens. All SS50 and SS150 specimens show a fiber slipping/pull-out failure mode with the typical load-slip curves, including the linear, nonlinear, and dynamic stages. The linear stage exhibits a complete bond between fiber and mortar, while the nonlinear stage indicates debonding occurring at the fiber-to-mortar interface and continues until the peak load. Then, complete debonding occurs, and the fiber pulls out from the mortar (the dynamic stage). For more information related to the pull-out mechanism, the reader is referred to [31,39]. The failure mode in SS200 is a combination of the fiber rupturing (for SS200-E60, SS200-E180) and slipping (for SS200-E300/360 and SS200-C0/360), as listed in Table A 1. The load-slip curves of the specimens with the fiber rupture show a linear and a partially nonlinear part until the peak load, followed by a sudden rupture of the fiber (Fig. 6). The failure of SS250 specimens is the fiber rupture (for SS250-C0 and SS250-E360) and fiber slipping (for SS250-E60/180/300 and SS250-C360) (see Table A 1). The fiber rupture occurs at the loaded end (inside the mortar or at the mortar interface)

due to reaching the applied load to the fiber tensile strength. Fiber rupturing shows that the bond strength at the interface of the fiber-to-mortar was higher than the tensile strength of the steel fibers and caused fiber failure. In Table A 1, the peak load of all steel-based TRM specimens with fiber failure is close to the tensile strength of the steel fiber (2819 MPa or 1517 N, as listed in Table 2). In general, in all embedded lengths, the control samples show a deterioration of bond performance with time (comparing the load-slip curves of C0 with C360 in Fig. 6). This observation is in line with that reported in [27]. The FT exposure, however, has different effects on specimens with different embedded lengths. For example, the load-slip curves of SS50-E and SS200-E specimens get flattered by increasing the number of cycles. In contrast, SS150-E and SS250-E show the opposite trend. Additionally, a few load-slip curves of steel-based TRM specimens (SS50-C360, SS150-C360, and SS200-E360) show a load drop after reaching peak load, followed by a slip-hardening effect (see Fig. 6). The fiber-to-mortar bond in a TRM composite with a high adhesion must be broken before the dynamic stage can begin. The load drop occurs when the load required to debond the fiber is higher than the frictional resistance after complete debonding, resulting in an unstable debonding [40]. In addition, slip hardening occurs due to increasing friction stress between the fiber and the mortar at the dynamic stage, as reported in [39].

The changes of the peak load (P_P), the debonding energy (E_{deb}), and the pull-out energy (E_{po}) with exposure are presented in Fig. 7 (the average values are also reported in Table A 1). E_{deb} and E_{po} are defined as the area under the load-slip curve until the peak load and from the peak load until the end, respectively. It should be mentioned that E_{po} is not calculated for SS250-E360 and SS250-C0 as the fibers failed at the peak load (see Fig. 6d). All pull-out parameters show, in general, a gradual decrement from 0 to 360 cycles under both the control and the FT conditions, as shown in Fig. 7. To better understand the effect of mortar age and FT conditions on the bond parameters, the difference (in percentage) between the average results at 360 cycles (C360 and E360) and the control specimens at 0 cycles (C0) are presented in Table A 1. It can be inferred that the bond parameters are deteriorated equally under both conditions, showing the proposed FT condition was not harsh enough. It seems other parameters cause the bond degradation to occur in both conditions, such as the long-term shrinkage effect by forming micro cracks at the bond interface. Continuing hydration (as mentioned in section 3.1) may lead to chemical shrinkage due to a reduction in the hydration volume of anhydrous compounds [41]. This output should be further investigated in future studies.

3.2.2 *Glass-reinforced mortar*

The average of pull-out response curves obtained for the glass-based TRMs with different bond lengths is presented in Fig. 8. Besides, Table A 2 presents the failure of these specimens. The load-slip curves of GS50 specimens includes the linear and nonlinear part until reaching the first peak load, followed by slip hardening effect and then decreasing load. These specimens generally fail under yarn slipping/pull-out mode though tensile rupture of the yarns occurs in GS50-E60/180 and GS50-C0 specimens at the dynamic stage. The failure of GS75 specimens is yarn slipping followed by rupturing. This observation is also supported by their load-slip curves, where the yarn slipped until reaching peak load and then ruptured at the dynamic stage. Meanwhile, GS100 samples are failed by fiber rupturing, so their load-slip curves only include the linear and nonlinear parts until a peak load is reached.

Load-slip curves show a decrease in bond performance of GS50 specimens. So, as the FT cycle or mortar age increases, the load-slip curve of GS50 specimens becomes flatter and the slip hardening effect is reduced due to the decrease in the friction stress at the bond interface. In contrast, other glass-based TRMs (GS75 and GS100) appear to show better performance with an increase in mortar age, both under the control and the FT conditions. This observation finds that both conditions have an adverse effect on the glass-based TRM when the bond length is equal to or less than the effective bond length (50 mm based on [32]), where the load slip curve is flattened by increasing the number of cycles. However, the development length in tension does not decrease for longer embedded lengths (75 and 100 mm), as the load-slip curves increase after 360 FT cycles. Fig. 9 shows the key parameters of the individual pull-out specimens with the regression line to show the general behavior of the glass-based TRM under the FT conditions. Since tensile rupture occurs at the peak load in GS75 and GS100 specimens, E_{po} is not presented for these specimens. Also, Table A 2 presents the difference between the FT and the control samples after 360 cycles with respect to the control conditions (C0), for a better analysis. The results show that the pull-out parameters of the GS50 specimens decrease under both conditions, compared to the GS75 and GS100 specimens showing an increase in the bond parameters. Due to the same decrease in pull-out parameters of GS50 specimens under both conditions, the proposed FT condition does not affect the bond behavior. Instead, it seems that a sort of bond deterioration by forming micro-cracks at the bond interface has occurred. One possible explanation is the negative impact of mortar hydration on the bond behavior of GS50 specimens, which continues until the end of the tests at

both conditions (see section 3.1). This negative effect can manifest in the form of chemical shrinkage or notching of the yarn surface due to the formation of precipitates [23]. Future studies need to explore this output more thoroughly. On the other hand, the mortar hydration does not affect the pull-out parameters of GS75 and GS100 specimens, which can be due to the longer embedded length of these specimens than GS50 specimens.

3.2.3 Comparison between steel and glass-based TRMs

To compare the behavior of steel and glass-based TRM under FT conditions, the results of SS50-E and GS50-E with equal bond lengths are selected. Generally, the steel-based TRMs (SS50-E) show a better performance than the glass-based TRMs (GS50-E) under the considered FT conditions. Comparing the load-slip curves of GS50 and SS50 specimens confirms this observation. In this way, glass-based TRMs show wide curves at the beginning of exposure, and by increasing the number of FT cycles, they become narrow and flat. On the other hand, the steel-based TRMs show wide curves at all cycles and only decrease at the end of the exposure. Besides, Fig. 10 compares the pull-out parameters of SS50-E and GS50-E specimens, in which standard deviations are presented by the error bar. The results show that the peak load (P_F) and the pull-out energy (E_{po}) of both systems are approximately equal (by considering the error bar). However, the debonding energy (E_{deb}) of SS50-E is higher than the GS50-E one due to the different transitions between the nonlinear and dynamic stages at these specimens.

3.3 Effect of textile configuration

3.3.1 Steel-reinforced mortar

The failure mode of SG150 specimens (with two cords) is generally fiber rupturing under the control and the FT conditions; however, SG150-C0 specimens show fiber slipping, as presented in Table A 3. Also, SG'150 specimens (with four cords) fail due to fiber slipping/pull-out under both conditions. The results also show that the failure modes of SG150 and SG'150 do not change from the control to the exposed specimens for the suggested period, like the single steel fiber specimens (SS150). The average of load-slip curves of both SG150 and SG'150 specimens are presented in Fig. 11. The pull-out response of SG150 specimens includes the linear and nonlinear stages, and by reaching the peak load, the load drops suddenly due to the fiber rupturing. On the other hand, the load-slip curves of SG'150 specimens show a typical pull-out curve.

Compared to SS150 specimens, the pull-out response of SG'150 samples (with four cords) shows the load decreasing with a steep slope after peak load under the control and the FT conditions. Increasing the number of fibers results in a decrease in the load carried by each fiber, which is due to the fiber volume fraction effect [42]. In addition, the pull-out response of the SG'150-C and SG'150-E specimens decreases by increasing the mortar age or increasing the number of the FT cycles, as shown in Fig. 11. In contrast to SS150 and SG'150, there are no changes from the load-slip curve of the SG150-C to SG150-E specimens.

The pull-out parameters of the individual specimens under the control and the FT conditions are reported in in Fig. 12 and their average values are presented in Table A 3. Since tensile rupture occurs at the peak load in SG150 specimens, E_{po} is not presented for these specimens. The results display that the FT condition causes the pull-out parameters to decrease slightly in SG150-E and SG'150-E specimens (although the P_p of the SG150-E increases slightly). However, in group fibers (SG150 and SG'150), bond parameters decrease less than those in single fibers (SS150) under freeze-thaw conditions. The difference of the bond parameters between the freezing-thawing exposure (E360) and the control specimens (C0), as well as between C360 and C0 specimens, shows that the FT condition does not affect the bond parameters of SG150 and SG'150 samples, see Table A 3. Again, the effects of chemical shrinkage on bond degradation can be emphasized further here due to continuing mortar hydration, as shown in section 3.1.

3.3.2 *Glass-reinforced mortar*

Fig. 13 shows the average load-slip curves of GT50 (with transverse yarns) and GG50 (2 group yarns) specimens under both the control and the FT conditions. In addition, Table A 4 reports their failure mode. All GT50 specimens fail under yarn slipping/pull-out followed by rupturing. This observation is supported by their load-slip curves, including the linear, nonlinear, and partially dynamic stages. A similar failure mode also is observed for all GG50 specimens, except GG50-C360 failed by tensile rupture when the peak load was reached. A comparison among the load-slip curves of GT50, GG50, and GS50 illustrates the positive effect of transverse elements, so the pull-out curves of GT50 and GG50 do not show load decreasing after peak load (dynamic stage). The load-slip curves of the control specimens (GT50-C and GG50-C) show that the pull-out response improves by increasing the mortar age, in contrast with the GS50-C specimens. Like GS50-E, the FT condition slightly declines the load-slip curves of GT50-E and GG50-E.

The key characteristics of the pull-out response of the individual GT50 and GG50 specimens are presented in Fig. 14 (see Table A 4 for the average of the pull-out parameters at each cycle). Since tensile rupture occurs at the peak load in several GG50 specimens, E_{po} is not presented for these specimens in Fig. 14c. Under the control condition, P_P of the GT50-C and GG50-C shows an incremental trend by increasing the mortar age though other pull-out parameters decline. Besides, a comparison between the GT50-C and GG50-C shows that the key characteristics of GG50-C specimens are higher than the pull-out parameters of GT50-C specimens. This observation reveals that fabric mesh influences the yarn-to-mortar bond behavior more than the single yarn with the transverse elements, even at different mortar ages.

Similar to the single glass-based TRM (GS50), the FT condition decreases the pull-out parameters in GG50-E, as shown in Fig. 14. However, GT50 specimens show an increasing trend under the FT conditions. Table A 4 also presents the difference of the bond parameters between the freezing-thawing exposure (E360) and the control (C0) specimens, as well as C360 and C0 specimens. The outcomes illustrate that under both conditions, the bond properties of GT50 specimens improve. Meanwhile, the outcomes display that the FT conditions lead to a considerable decrement of all pull-out parameters in GG50-E360 specimens, in contrast to GG50-C360. As a result of this observation, it is apparent that glass fabric configuration affects the pull-out response, resulting in different bond behavior under FT conditions. Therefore, studying from single to mesh configurations of this type of fiber is crucial to better understand their behavior.

4 Conclusions

The effect of freeze-thaw (FT) conditions on the micro-mechanical response of steel and glass-based TRM composites was examined in this study. This research included investigating the mortar strength changes and the bond performance as a function of embedded length, number of yarns/cords, use of transverse fibers, and age. In general, the following conclusions can be drawn:

- The mechanical properties of the lime-based mortar used in this study remained constant (with a slight improvement) under both the control and FT conditions. This observation shows that the detrimental effect of the considered FT conditions was less than the mortar hydration positive effect on the strength. This can also be due to the fact that although 90% RH was considered in the FT exposure conditions, this condition might not have been

sufficiently high for saturating the samples until a critical level in the time frame of the experimental tests.

- As expected, the mechanical properties of the glass fibers were not affected by the FT conditions. However, the tensile strength of steel fibers decreased slightly.
- The pull-out response of the steel-based TRMs with different bond lengths generally deteriorated both in the control and under the FT conditions. The highest deterioration was observed in the 50 mm bonded length samples under FT conditions. However, the bond deterioration trend decreased by increasing the bond length. This was expected as with an increment of the bond length, the importance of local bond deterioration becomes less significant.
- The effect of FT conditions on the glass-based TRM varied with different embedded lengths. While 50 mm embedded length samples showed deterioration of the bond strength, 75 mm and 100 mm samples showed an enhancement of the bond strength (peak load and debonding energy). A similar observation was also found for the specimens cured in the lab conditions.
- The effect of FT conditions on the pull-out response of the group steel-based TRM was significantly different than that of the single cord samples. While both control and FT conditions led to enhancement of the peak load in the samples reinforced with two cords, those conditions caused deterioration in single and four cord samples. While this requires further investigations, it shows the importance of considering the group behavior in closely distanced fabrics.
- The yarn configuration was also found to be important in glass-based TRMs (in which a bidirectional fabric was used). While the bond behavior of the specimens with transverse yarns enhanced under the FT conditions, the samples with group yarns showed a considerable deterioration similar to those observed in single yarn samples.

These observations show the importance of considering the actual architecture of the fabrics in experimental specimens for evaluating the mechanical and durability performance of TRM composites. Also, consideration of other FT exposure conditions is suggested to be considered in future studies.

Acknowledgments

This work was partly financed by FCT/MCTES through national funds (PIDDAC) under the R&D Unit Institute for Sustainability and Innovation in Structural Engineering (ISISE), under reference UIDB/04029/2020. The support to the first author through grant agreement SFRH/BD/131282/2017, provided by FCT- Foundation for Science and Technology, is kindly acknowledged.

5 References

- [1] Z. Zhou, P. Walker, D. D'Ayala, Strength characteristics of hydraulic lime mortared brickwork, *Proc. Inst. Civ. Eng. - Constr. Mater.* 161 (2008) 139–146. <https://doi.org/10.1680/coma.2008.161.4.139>.
- [2] C. Pellegrino, J. Sena-Cruz, eds., Design procedures for the use of composites in strengthening of reinforced concrete structures- State-of-the-Art report of the RILEM technical committee 234-DUC, RILEM, Springer, 2016. <https://doi.org/10.1007/978-94-017-7336-2> ISSN.
- [3] B. Mobasher, *Mechanics of Fiber and Textile Reinforced Cement Composites*, Taylor & Francis Group, London- New York, 2012.
- [4] A. Moropoulou, A. Bakolas, P. Moundoulas, E. Aggelakopoulou, S. Anagnostopoulou, Strength development and lime reaction in mortars for repairing historic masonries, *Cem. Concr. Compos.* 27 (2005) 289–294. <https://doi.org/10.1016/j.cemconcomp.2004.02.017>.
- [5] C. Montoya, J. Lanas, M. Arandigoyen, I. Navarro-Blasco, P.J. García Casado, J.I. Alvarez, Study of ancient dolomitic mortars of the church of Santa María de Zamarce in Navarra (Spain): Comparison with simulated standards, *Thermochim. Acta.* 398 (2003) 107–122. [https://doi.org/10.1016/S0040-6031\(02\)00321-0](https://doi.org/10.1016/S0040-6031(02)00321-0).
- [6] X. Wang, C.C. Lam, V.P. Iu, Bond behaviour of steel-TRM composites for strengthening masonry elements: Experimental testing and numerical modelling, *Constr. Build. Mater.* 253 (2020) 119157. <https://doi.org/10.1016/j.conbuildmat.2020.119157>.
- [7] A. Bellini, M. Bovo, C. Mazzotti, Experimental and numerical evaluation of fiber-matrix interface behaviour of different FRCM systems, *Compos. Part B Eng.* 161 (2019) 411–426. <https://doi.org/10.1016/j.compositesb.2018.12.115>.
- [8] S. De Santis, H.A. Hadad, F. De Caso y Basalo, G. de Felice, A. Nanni, Acceptance criteria for tensile characterization of fabric-reinforced cementitious matrix systems for concrete and masonry repair, *J. Compos. Constr.* 22 (2018) 04018048. [https://doi.org/10.1061/\(ASCE\)CC.1943-5614.0000886](https://doi.org/10.1061/(ASCE)CC.1943-5614.0000886).
- [9] Z. Dong, M. Deng, C. Zhang, Y. Zhang, H. Sun, Tensile behavior of glass textile reinforced mortar (TRM) added with short PVA fibers, *Constr. Build. Mater.* 260 (2020) 119897. <https://doi.org/10.1016/j.conbuildmat.2020.119897>.
- [10] S. Mazzuca, H.A. Hadad, L. Ombres, A. Nanni, Mechanical Characterization of Steel-Reinforced Grout for Strengthening of Existing Masonry and Concrete Structures, *J. Mater. Civ. Eng.* 31 (2019) 04019037. [https://doi.org/10.1061/\(ASCE\)MT.1943-5533.0002669](https://doi.org/10.1061/(ASCE)MT.1943-5533.0002669).
- [11] Z. Mesticou, L. Bui, A. Junes, A. Si Larbi, A.S. Larbi, Experimental investigation of tensile fatigue behaviour of Textile- Reinforced Concrete (TRC): Effect of fatigue load and strain rate, *Compos. Struct.* 160 (2017) 1136–1146. <https://doi.org/10.1016/j.compstruct.2016.11.009>.
- [12] A. Dalalbashi, B. Ghiassi, D. V. Oliveira, Textile-to-mortar bond behaviour in lime-based textile reinforced mortars, *Constr. Build. Mater.* 227 (2019) 116682. <https://doi.org/10.1016/j.conbuildmat.2019.116682>.
- [13] W. Bramehuber, ed., RILEM TC 201-TRC: Textile reinforced concrete- state-of-the-art, RILEM, Bagneux, 2006.
- [14] E. Franzoni, M. Santandrea, C. Gentilini, A. Fregni, C. Carloni, The role of mortar matrix in the bond behavior and salt crystallization resistance of FRCM applied to masonry, *Constr. Build. Mater.* 209 (2019) 592–605. <https://doi.org/10.1016/j.conbuildmat.2019.03.059>.
- [15] J. Donnini, Durability of glass FRCM systems: Effects of different environments on mechanical properties, *Compos. Part B.* (2019) 107047. <https://doi.org/10.1016/j.compositesb.2019.107047>.
- [16] B. Ghiassi, Mechanics and durability of textile reinforced mortars: a review of recent advances and open

- issues, RILEM Tech. Lett. 4 (2019) 130–137. <https://doi.org/10.21809/rilemtechlett.2019.99>.
- [17] M. Alma'aitah, B. Ghiassi, A. Dalalbashi, Durability of textile reinforced concrete: Existing knowledge and current gaps, Appl. Sci. 11 (2021) 1–10. <https://doi.org/10.3390/app11062771>.
- [18] O. Homoro, X.H. Vu, E. Ferrier, Experimental and analytical study of the thermo-mechanical behaviour of textile-reinforced concrete (TRC) at elevated temperatures: Role of discontinuous short glass fibres, Constr. Build. Mater. 190 (2018) 645–663. <https://doi.org/10.1016/j.conbuildmat.2018.09.142>.
- [19] S. De Santis, G. de Felice, Steel reinforced grout systems for the strengthening of masonry structures, Compos. Struct. 134 (2015) 533–548. <https://doi.org/10.1016/j.compstruct.2015.08.094>.
- [20] S. Liu, P. Rawat, Z. Chen, S. Guo, C. Shi, D. Zhu, Pullout behaviors of single yarn and textile in cement matrix at elevated temperatures with varying loading speeds, Compos. Part B Eng. 199 (2020) 108251. <https://doi.org/10.1016/j.compositesb.2020.108251>.
- [21] I.G. Colombo, M. Colombo, M. Prisco, Tensile behavior of textile reinforced concrete subjected to freezing-thawing cycles in un-cracked and cracked regimes, Cem. Concr. Res. 73 (2015) 169–183. <https://doi.org/10.1016/j.cemconres.2015.03.001>.
- [22] B.Y. Pekmezci, E. Arabaci, C. Ustundag, Freeze-thaw durability of lime based FRCM systems for strengthening historical masonry, Key Eng. Mater. 817 KEM (2019) 174–181. <https://doi.org/10.4028/www.scientific.net/KEM.817.174>.
- [23] M. De Munck, M. El Kadi, E. Tsangouri, J. Vervloet, S. Verbruggen, J. Wastiels, T. Tysmans, O. Remy, Influence of environmental loading on the tensile and cracking behaviour of textile reinforced cementitious composites, Constr. Build. Mater. 181 (2018). <https://doi.org/10.1016/j.conbuildmat.2018.06.045>.
- [24] A. Nobili, C. Signorini, On the effect of curing time and environmental exposure on impregnated Carbon Fabric Reinforced Cementitious Matrix (CFRCM) composite with design considerations, Compos. Part B. 112 (2017) 300–313. <https://doi.org/10.1016/j.compositesb.2016.12.022>.
- [25] D. Arboleda, S. Babaeidarabad, C.D. Hays, A. Nanni, Durability of fabric reinforced cementitious matrix (FRCM) composites, in: 7th. Int. Conf. FRP Compos. Civ. Eng. (CICE 2014), Vancouver, 2014: pp. 1–6.
- [26] J. Donnini, F. Bompadre, V. Corinaldesi, Tensile behavior of a glass FRCM system after different environmental exposures, Processes. 8 (2020). <https://doi.org/10.3390/pr8091074>.
- [27] A. Dalalbashi, B. Ghiassi, D. V. Oliveira, Aging of lime-based TRM composites under natural environmental conditions, Constr. Build. Mater. 270 (2021). <https://doi.org/10.1016/j.conbuildmat.2020.121853>.
- [28] ASTM C109/C109M-05, Standard test method for compressive strength of hydraulic cement mortars (Using 2-in. or [50-mm] Cube Specimens), 2005. https://doi.org/10.1520/C0109_C0109M-05.
- [29] BS EN 1015-11, Methods of test for mortar for masonry. Determination of flexural and compressive strength of hardened mortar, 1999.
- [30] BS EN 12390-13, Testing hardened concrete. Determination of secant modulus of elasticity in compression, 2013.
- [31] A. Dalalbashi, B. Ghiassi, D.V. Oliveira, A. Freitas, Effect of test setup on the fiber-to-mortar pull-out response in TRM composites: experimental and analytical modeling, Compos. Part B Eng. 143 (2018) 250–268. <https://doi.org/10.1016/j.compositesb.2018.02.010>.
- [32] A. Dalalbashi, B. Ghiassi, D.V. Oliveira, A. Freitas, Fiber-to-mortar bond behavior in TRM composites: effect of embedded length and fiber configuration, Compos. Part B Eng. 152 (2018) 43–57. <https://doi.org/10.1016/j.compositesb.2018.06.014>.
- [33] B. Ghiassi, D. V Oliveira, P.B. Lourenço, Hygrothermal durability of bond in FRP-strengthened masonry, (2014) 2039–2050. <https://doi.org/10.1617/s11527-014-0375-7>.
- [34] R.M.H. Lawrence, T.J. Mays, P. Walker, D.D. Ayala, Determination of carbonation profiles in non-hydraulic lime mortars using thermogravimetric analysis, Thermochim. Acta. 444 (2006) 179–189. <https://doi.org/10.1016/j.tca.2006.03.002>.
- [35] S.H. Kang, Y.H. Kwon, J. Moon, Controlling the hydration and carbonation in lime-based materials: Advantage of slow carbonation in CO₂ curable construction materials, Constr. Build. Mater. 249 (2020) 118749. <https://doi.org/10.1016/j.conbuildmat.2020.118749>.
- [36] Ö. Cizer, K. Van Balen, D. Van Gemert, Competition between hydration and carbonation in hydraulic lime and lime-pozzolana mortars, Adv. Mater. Res. 133–134 (2010) 241–246. <https://doi.org/10.4028/www.scientific.net/AMR.133-134.241>.
- [37] A. El-Turki, R.J. Ball, S. Holmes, W.J. Allen, G.C. Allen, Environmental cycling and laboratory testing to evaluate the significance of moisture control for lime mortars, Constr. Build. Mater. 24 (2010) 1392–1397. <https://doi.org/10.1016/j.conbuildmat.2010.01.019>.

- [38] J. Lanas, J. Perez Bernal, M.A. Bello, J.I. Alvarez Galindo, Mechanical properties of natural hydraulic lime-based mortars, *Cem. Concr. Res.* 34 (2004) 2191–2201. <https://doi.org/10.1016/j.cemconres.2004.02.005>.
- [39] A. Dalalbashi, B. Ghiassi, D. V. Oliveira, Textile-to-mortar bond behavior: An analytical study, *Constr. Build. Mater.* 282 (2020) 122639. <https://doi.org/10.1016/j.conbuildmat.2021.122639>.
- [40] W.P. Boshoff, V. Mechtcherine, G.P.A.G. van Zijl, Characterising the time-dependant behaviour on the single fibre level of SHCC: Part 2: The rate effects on fibre pull-out tests, *Cem. Concr. Res.* 39 (2009) 787–797. <https://doi.org/10.1016/j.cemconres.2009.06.006>.
- [41] A. Duran, J.M. Fernández, J.I. Alvarez, Long-term mechanical resistance and durability of air lime mortars with large additions of nanosilica, *Constr. Build. Mater.* 58 (2014) 147–158. <https://doi.org/10.1016/j.conbuildmat.2014.02.030>.
- [42] A. Pacios, C. Ouyang, S.P. Shah, Rate effect on interfacial response between fibres and matrix, *Mater. Struct.* 28 (1995) 83–91. <https://doi.org/10.1007/BF02473175>.

6 Appendix

Table A 1. Changes of bond properties in steel-based TRM with different embedded lengths*.

Embedded length [mm]	Name	P _p [N]	P _p /P _{p,C0} -1 [%]	E _{deb} [N.mm]	E _{deb} /E _{deb,C0} -1 [%]	E _{po} [N.mm]	E _{po} /E _{po,C0} -1 [%]	Failure	Number of specimens
50	SS50-C0	587.9 (14)	-	1545.8 (17)	-	4209.9 (14)	-	slip	4
	SS50-E60	412.5 (13)	-	1197.3 (38)	-	2495.4 (15)	-	slip	4
	SS50-E180	584.1 (22)	-	1102 (34)	-	4314 (23)	-	slip	5
	SS50-E300	349.8 (29)	-	798.8 (30)	-	3110 (30)	-	slip	5
	SS50-E360	420.3 (22)	-29	1168.6 (49)	-24	2859.5 (16)	-32	slip	5
	SS50-C360	535.6 (15)	-9	99.1 (30)	-94	5445.5 (14)	29	slip	4
150	SS150-C0	1279.7 (11)	-	3810.1 (25)	-	9816 (13)	-	slip	5
	SS150-E60	1301.3 (22)	-	2892.6 (11)	-	6755.2 (15)	-	slip	5
	SS150-E180	1032.6 (26)	-	1444.8 (39)	-	8503.1 (23)	-	slip	5
	SS150-E300	1087.4 (18)	-	2578.7 (25)	-	8186.3 (18)	-	slip	5
	SS150-E360	1389.4 (7)	9	3772.8 (42)	-1	10883.5 (25)	11	slip	4
	SS150-C360	874.6 (19)	-32	562.5 (40)	-85	9698.4 (10)	-1	slip	5
200	SS200-C0	1164.2 (26)	-	4033.4 (39)	-	7747.7 (21)	-	slip	5
	SS200-E60	1622.8 (2)	-	2051 (15)	-	-	-	rupture	4
	SS200-E180	1622.2 (1)	-	1994.8 (16)	-	-	-	rupture	5
	SS200-E300	1289.4 (13)	-	3759.2 (22)	-	9540.4 (13)	-	slip	5
	SS200-E360	980.9 (11)	-16	1021.1 (25)	-75	8616.4 (6)	11	slip	4
	SS200-C360	923.3 (12)	-21	3140.4 (38)	-22	7374 (14)	-5	slip	5
250	SS250-C0	1642.5 (3)	-	3874.1 (24)	-	-	-	rupture	4
	SS250-E60	1568.1 (7)	-	3742.7 (43)	-	11200.6 (2)	-	slip	5
	SS250-E180	1526.7 (4)	-	2798.7 (13)	-	12797.3 (9)	-	slip	5
	SS250-E300	1166.9 (11)	-	3446.9 (12)	-	8481.2 (3)	-	slip	5
	SS250-E360	1690.2 (2)	3	2456.4 (24)	-37	-	-	rupture	5
	SS250-C360	1507.3 (10)	-8	4541.4 (16)	17	11538.9 (7)	-	slip	5

*Coefficients of variation in percentage are provided inside parentheses.

P_p: Peak load; E_{deb}: Debonding energy; E_{po}: Pull-out energy.

Table A 2. Changes of bond properties in glass-based TRM with different embedded lengths*.

Embedded length [mm]	Name	P _p [N]	P _p /P _{p,C0} -1 [%]	E _{deb} [N.mm]	E _{deb} /E _{deb,C0} -1 [%]	E _{po} [N.mm]	E _{po} /E _{po,C0} -1 [%]	Failure	Number of specimens
50	GS50-C0	502.3 (14)	-	208.1 (9)	-	4161.9 (34)	-	slip	4
	GS50-E60	513.5 (6)	-	105.6 (25)	-	4286.1 (27)	-	slip	4
	GS50-E180	502.4 (14)	-	191.4 (26)	-	4339.0 (3)	-	slip	4
	GS50-E300	329.2 (11)	-	90.6 (24)	-	3748.3 (26)	-	slip	4
	GS50-E360	308.0 (10)	-39	31.5 (15)	-85	2573.8 (13)	-38	slip	4
	GS50-C360	308.4 (24)	-39	63.3 (25)	-70	2776.0 (25)	-33	slip	4
75	GS75-C0	613.1 (6)	-	301.7 (17)	-	-	-	slip followed by rupture	5
	GS75-E60	569.3 (18)	-	258.3 (37)	-	-	-	slip followed by rupture	4
	GS75-E180	545.4 (14)	-	185.3 (27)	-	-	-	slip followed by rupture	4
	GS75-E300	576.8 (10)	-	171.1 (18)	-	-	-	slip followed by rupture	5
	GS75-E360	724.4 (4)	18	1206 (14)	300	-	-	slip followed by rupture	5
	GS75-C360	695.6 (17)	13	294.8 (32)	-2	-	-	slip followed by rupture	5
100	GS100-C0	722.5 (7)	-	592.9 (32)	-	-	-	rupture	5
	GS100-E60	827.9 (9)	-	926.3 (36)	-	-	-	rupture	5
	GS100-E180	701.5 (4)	-	482.5 (15)	-	-	-	rupture	4
	GS100-E300	830.7 (8)	-	699.8 (16)	-	-	-	rupture	5
	GS100-E360	871.3 (7)	21	785.5 (19)	32	-	-	rupture	5
	GS100-C360	840.9 (6)	16	605.3 (17)	2	-	-	rupture	5

*Coefficients of variation in percentage are provided inside parentheses.

P_p: Peak load; E_{deb}: Debonding energy; E_{po}: Pull-out energy.

512

Table A 3. Changes of bond properties in steel-based TRM with different fiber configurations*.

Fiber configuration	Name	P _p [N]	P _p /P _{p,C0} -1 [%]	E _{deb} [N.mm]	E _{deb} /E _{deb,C0} -1 [%]	E _{po} [N.mm]	E _{po} /E _{po,C0} -1 [%]	Failure	Number of specimens
Two cords	SG150-C0	1489.2 (11)	-	2253 (37)	-	-	-	slip	5
	SG150-E60	1494.3 (5)	-	1915 (38)	-	-	-	rupture	5
	SG150-E180	1625.1 (1)	-	1901.9 (15)	-	-	-	rupture	5
	SG150-E300	1630.7 (5)	-	1919.4 (16)	-	-	-	rupture	5
	SG150-E360	1627.2 (5)	9	1832.4 (17)	-19	-	-	rupture	5
	SG150-C360	1536.1 (9)	3	1446.8 (15)	-36	-	-	rupture	4
Four cords	SG'150-C0	1304 (5)	-	1700 (19)	-	6441.7 (21)	-	slip	5
	SG'150-E60	1224.7 (5)	-	2019.1 (18)	-	7175.8 (12)	-	slip	5
	SG'150-E180	1424.6 (6)	-	1721 (15)	-	6279.6 (6)	-	slip	5
	SG'150-E300	1364.2 (7)	-	1883.8 (18)	-	7683 (4)	-	slip	5
	SG'150-E360	1231.3 (7)	-6	1918.2 (23)	13	6868.3 (17)	7	slip	5
	SG'150-C360	847.7 (14)	-35	1435.3 (16)	-16	5998.9 (8)	-7	slip	5

*Coefficients of variation in percentage are provided inside parentheses.

P_p: Peak load; E_{deb}: Debonding energy; E_{po}: Pull-out energy.

513

514

515

516

517

518

519

520

521

522

523

524

525

526

527

528

529

530

531

532

Table A 4. Changes of bond properties in glass-based TRM with different fiber configurations*.

Fiber configuration	Name	P _p [N]	P _p /P _{p,C0} -1 [%]	E _{deb} [N.mm]	E _{deb} /E _{deb,C0} -1 [%]	E _{po} [N.mm]	E _{po} /E _{po,C0} -1 [%]	Failure	Number of specimens
Single yarn+ transverse elements	GT50-C0	272.9 (17)	-	28.3 (35)	-	4026.1 (42)	-	slip	5
	GT50-E60	716.6 (10)	-	855.4 (56)	-	2794.5 (37)	-	slip	5
	GT50-E180	572.7 (11)	-	1041.1 (39)	-	-	-	slip	5
	GT50-E300	458.6 (17)	-	124 (27)	-	2352.5 (38)	-	slip	5
	GT50-E360	456.2 (12)	67	80.2 (22)	183	4733.5 (14)	18	slip	4
	GT50-C360	449.1 (26)	65	82.2 (59)	190	1771.1 (71)	-56	slip	4
Two group yarns	GG50-C0	641.9 (8)	-	2252.4 (34)	-	-	-	slip	5
	GG50-E60	605.1 (6)	-	3362.7 (12)	-	-	-	slip	5
	GG50-E180	383 (21)	-	71.0 (51)	-	2073 (44)	-	slip	5
	GG50-E300	368.1 (3)	-	44.0 (21)	-	5268.2 (6)	-	slip	4
	GG50-E360	401.0 (11)	-38	89.5 (30)	-96	5091.1 (18)	-	slip	5
	GG50-C360	796.0 (13)	24	1084.5 (30)	-52	-	-	rupture	5

*Coefficients of variation in percentage are provided inside parentheses.

P_p: Peak load; E_{deb}: Debonding energy; E_{po}: Pull-out energy.

533

534

535

536

537

538

539

540

541

Table 1. Experimental program.

Test	material	Fiber configuration	Bond length [mm]	Freeze-thaw cycles					Name	Number of specimens × cycles
				0	60	180	300	360		
Compressive	Mortar	-	-			*		*	-	5 × 7
Flexural	Mortar	-	-			*		*	-	5 × 5
Elastic modulus	Mortar	-	-			*		*	-	5 × 5
Tensile	Glass and steel fibers	-	-					*	-	5 × 3
Pull-out (embedded length)	Glass yarn and mortar	Single yarn	50					*	GS50-C0, GS50-C360, GS50-E60~GS50-E360	5 × 7
			75					*	GS75-C0, GS75-C360, GS75-E60~GS75-E360	5 × 7
			100					*	GS100-C0, GS100-C360, GS100-E60~GS100-E360	5 × 7
	Steel fiber and mortar	Single cord	50					*	SS50-C0, SS50-C360, SS50-E60~SS50-E360	5 × 7
			150					*	SS150-C0, SS150-C360, SS150-E60~SS150-E360	5 × 7
			200					*	SS200-C0, SS200-C360, SS200-E60~SS200-E360	5 × 7
			250					*	SS250-C0, SS250-C360, SS250-E60~SS250-E360	5 × 7
	Pull-out (fiber configuration)	Glass yarn and mortar	Single yarn + transverse Group (2 yarns)	50				*	GT50-C0, GT50-C360, GT50-E60~GT50-E360	5 × 7
								*	GG50-C0, GG50-C360, GG50-E60~GG50-E360	5 × 7
		Steel fiber and mortar	Group (2 cords)	150				*	SG150-C0, SG150-C360, SG150-E60~SG150-E360	5 × 7
								*	SG'150-C0, SG'150-C360, SG'150-E60~SG'150-E360	5 × 7

542

*Tested both control and exposed specimens; the grey cells indicate the performed tests.

543

544

Table 2. Mortar and fibers Mechanical properties*.

Strength [MPa]	Material	Control specimens corresponding to FT exposures cycles			Exposed specimens			
		C0	C180	C360	E60	E180	E300	E360
Compressive strength	Mortar	16.8 (11)	20 (12)	17.3 (10)	17.0 (10)	19.5 (5)	17.3 (2)	18.8 (3)
Flexural strength	Mortar	4.5 (2)	4.5 (12)	4.7 (5)	-	5.8 (5)	-	5.0 (5)
Elastic modulus	Mortar	6713 (6)	8280 (11)	8095 (10)	-	7593 (1)	-	7462 (12)
	Steel fiber	189340 (8)	-	-	-	-	-	173000 (2)
	Glass fiber	65940 (5)	-	-	-	-	-	70720 (3)
Tensile strength	Steel fiber	2972 (8)	-	-	-	-	-	2819 (1)
	Glass fiber	875 (13)	-	-	-	-	-	899 (5)

545

*Coefficient of variation of the results is given in percentage inside parentheses.

List of Figs.

Fig. 1. Schematic representation of the test program.

Fig. 2. Material characterization tests: (a) compressive test; (b) flexural test; (c) elastic modulus test; (d) fabric direct tensile test.

Fig. 3. Details of the pull-out specimens: (a) geometry of specimens; (b) steel fiber configuration; (c) glass fabric configurations; (d) test setup details.

Fig. 4. (a) Freeze-thaw exposure condition; (b) environmental lab condition.

Fig. 5. DTA curves in the 50-1000°C.

Fig. 6. Average of load-slip response of single steel fibers in different bond lengths: (a) SS50; (b) SS150; (c) SS200; (d) SS250.

Fig. 7. Pull-out parameters of single steel-based TRM in different bond lengths: (a) peak load; (b) debonding energy; (c) pull-out energy.

Fig. 8. Load-slip response of single glass fibers in different bond lengths: (a) GS50; (b) GS75; (c) GS100.

Fig. 9. Pull-out parameters of single glass-based TRM in different bond lengths: (a) peak load; (b) debonding energy; (c) pull-out energy.

Fig. 10. Comparison between pull-out parameters of glass and steel-based TRM in 50 mm bond length: (a) peak load; (b) debonding energy; (c) pull-out energy.

Fig. 11. Pull-out response of steel-based TRMs with different configurations: (a) SG150; (b) SG'150.

Fig. 12. Pull-out parameters of group steel-based TRM: (a) peak load; (b) debonding energy; (c) pull-out energy.

Fig. 13. Pull-out response of glass-based TRMs with different configurations: (a) GT50; (b) GG50.

Fig. 14. Pull-out parameters of single+ transverse and group glass-based TRM: (a) peak load; (b) debonding energy; (c) pull-out energy.

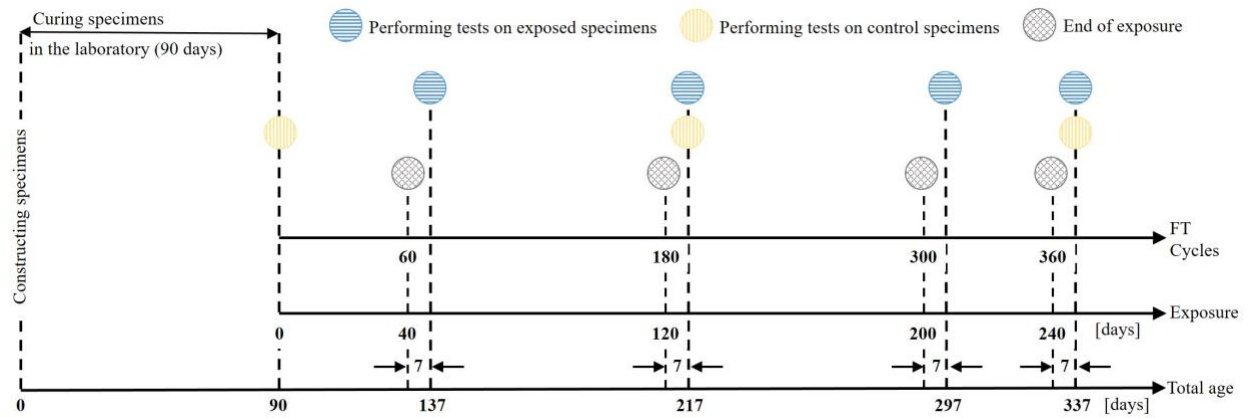
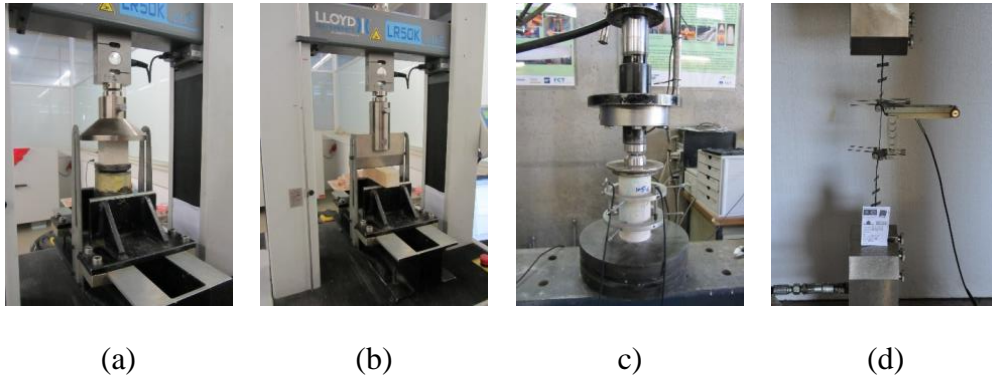
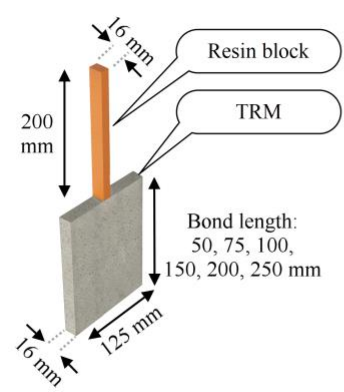


Fig. 1. Schematic representation of the test program.

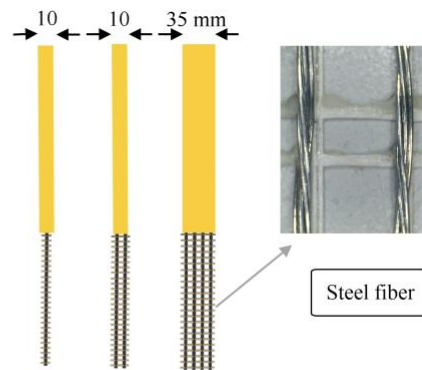
573



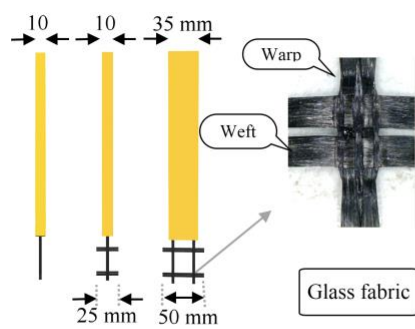
574 Fig. 2. Material characterization tests: (a) compressive test; (b) flexural test; (c) elastic modulus
575 test; (d) fabric direct tensile test.
576
577



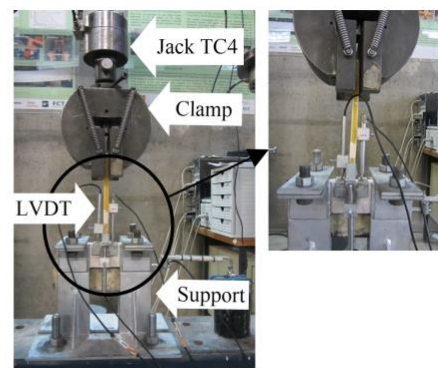
(a)



(b)



(c)



(d)

Fig. 3. Details of the pull-out specimens: (a) geometry of specimens; (b) steel fiber configuration; (c) glass fabric configurations; (d) test setup details.

582

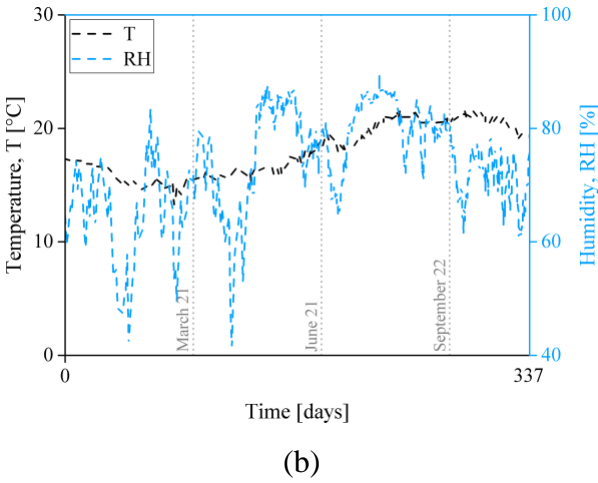
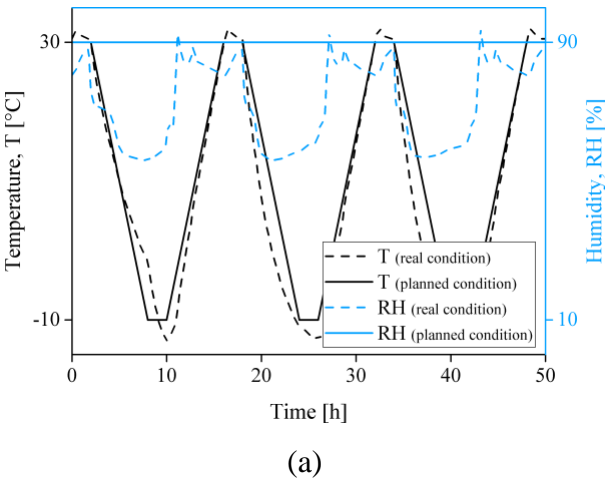


Fig. 4. (a) Freeze-thaw exposure condition; (b) environmental lab condition.

583

584

585

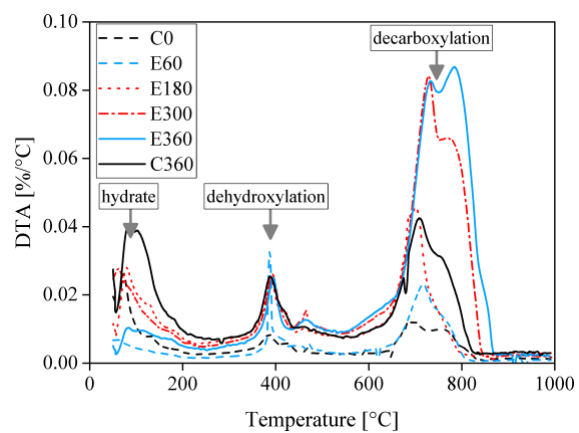
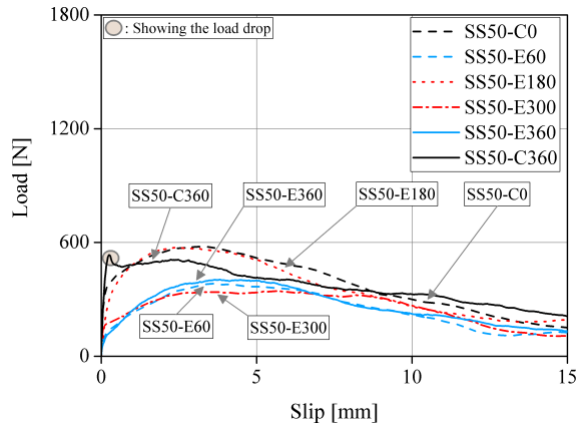
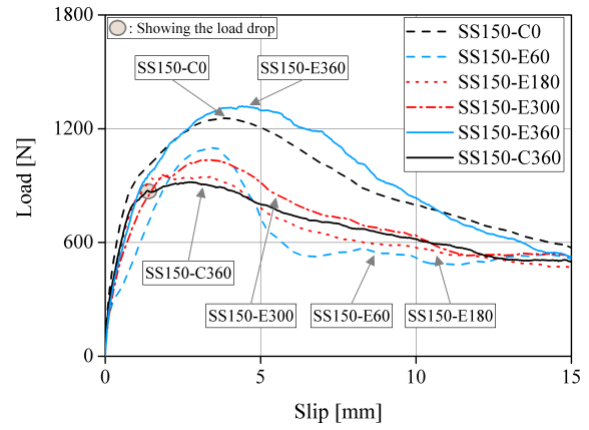


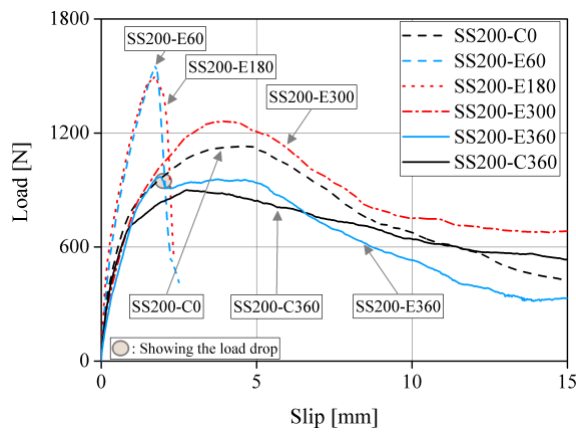
Fig. 5. DTA curves in the 50-1000°C.



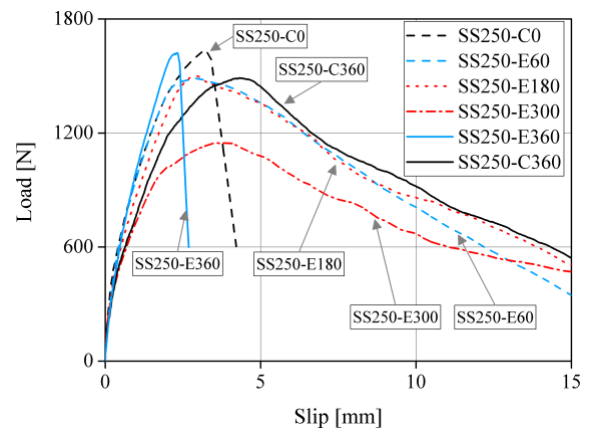
(a)



(b)



(c)



(d)

Fig. 6. Average of load-slip response of single steel fibers in different bond lengths: (a) SS50; (b) SS150; (c) SS200; (d) SS250.

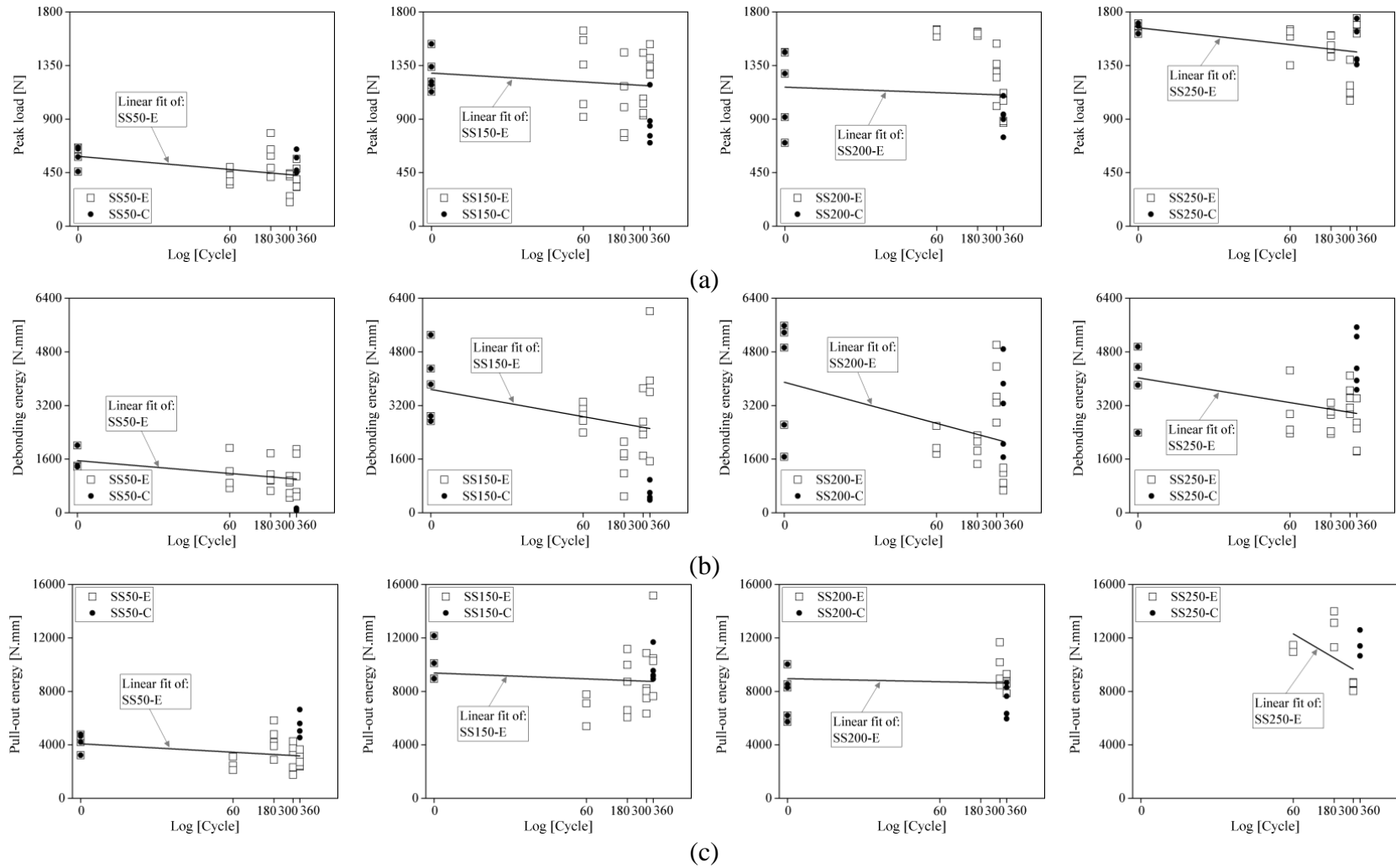
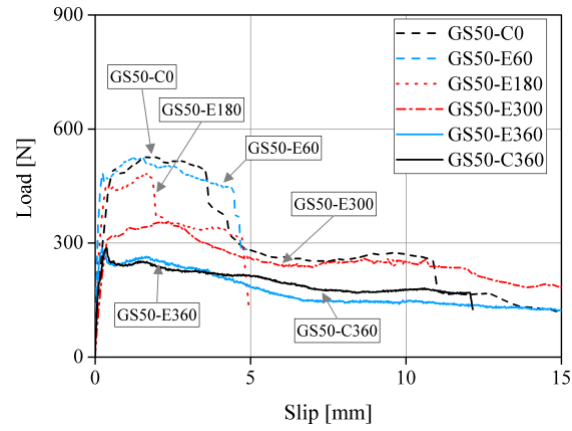
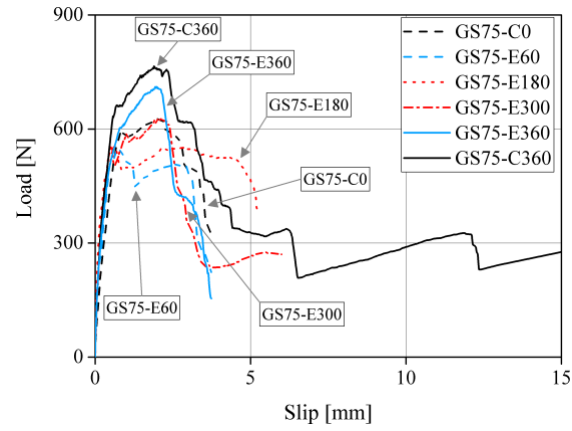


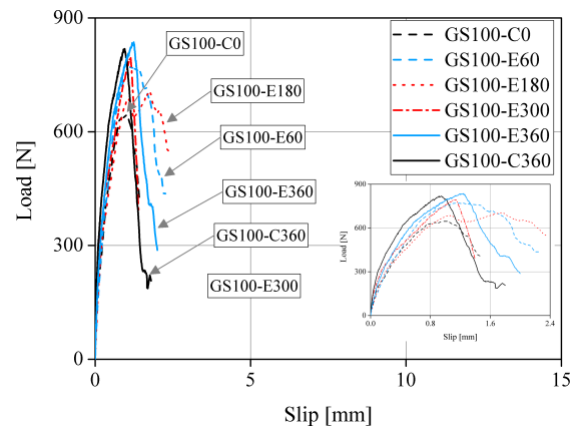
Fig. 7. Pull-out parameters of single steel-based TRM in different bond lengths: (a) peak load; (b) debonding energy; (c) pull-out energy.



(a)



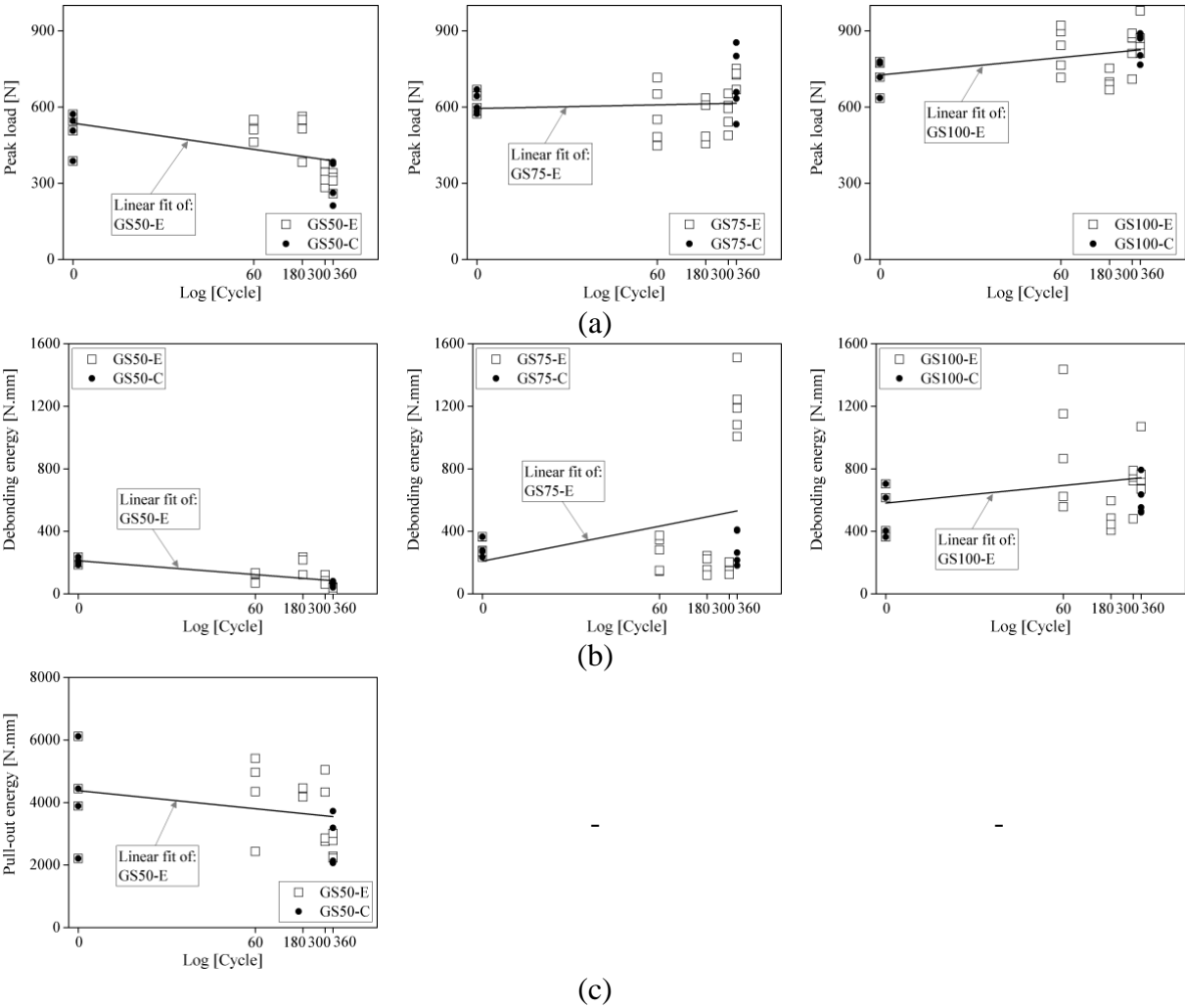
(b)



(c)

Fig. 8. Average of load-slip response of single glass fibers in different bond lengths: (a) GS50; (b) GS75; (c) GS100.

603



604 Fig. 9. Pull-out parameters of single glass-based TRM in different bond lengths: (a) peak load;
605 (b) debonding energy; (c) pull-out energy.
606

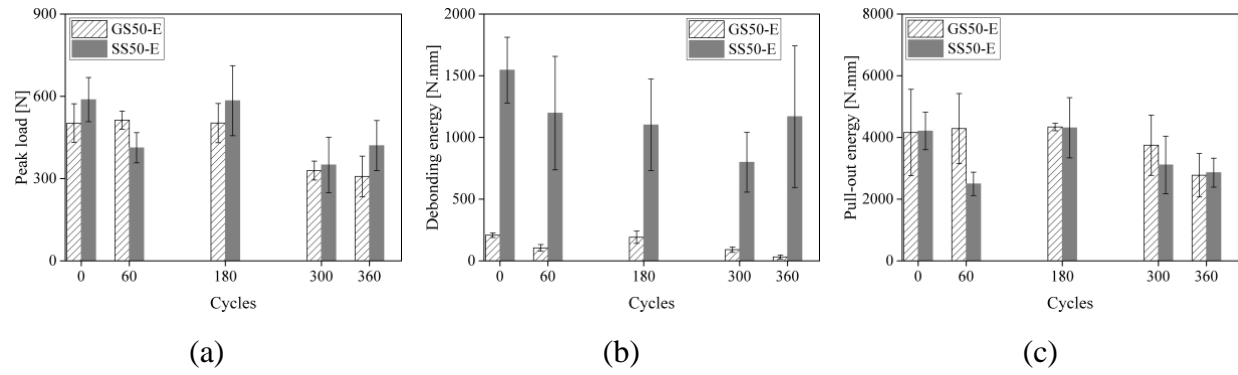
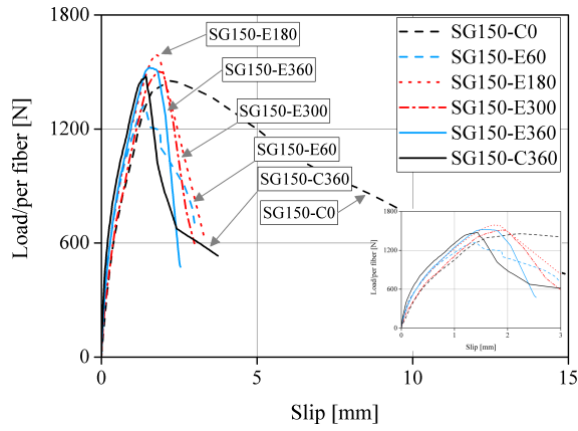
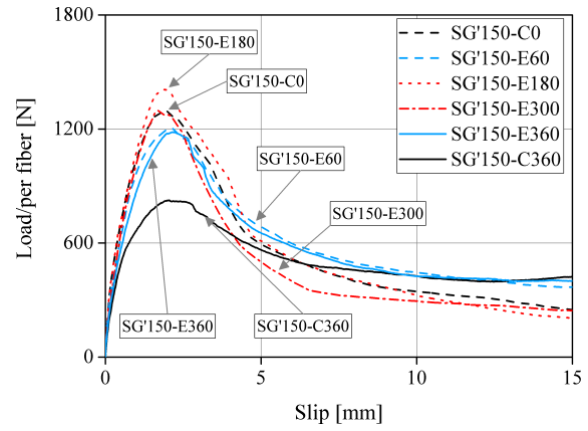


Fig. 10. Comparison between pull-out parameters of glass and steel-based TRM in 50 mm bond length: (a) peak load; (b) debonding energy; (c) pull-out energy.

612

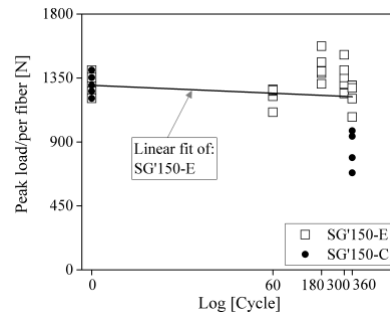
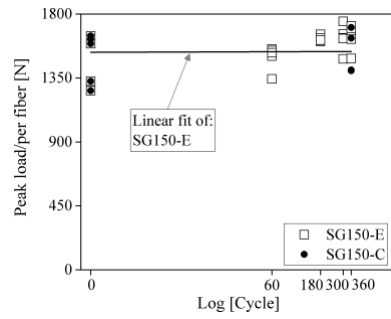


(a)

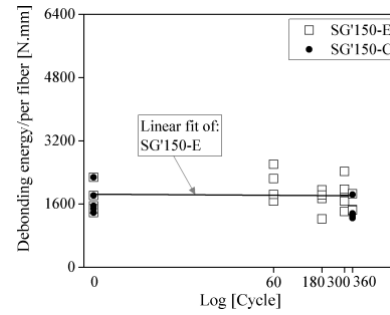
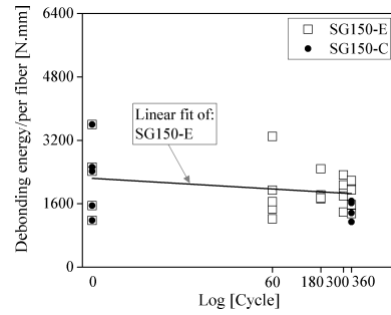


(b)

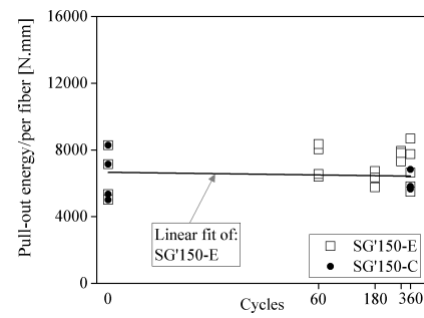
Fig. 11. Average of load-slip response of steel-based TRMs with different configurations: (a) SG150; (b) SG'150.



(a)



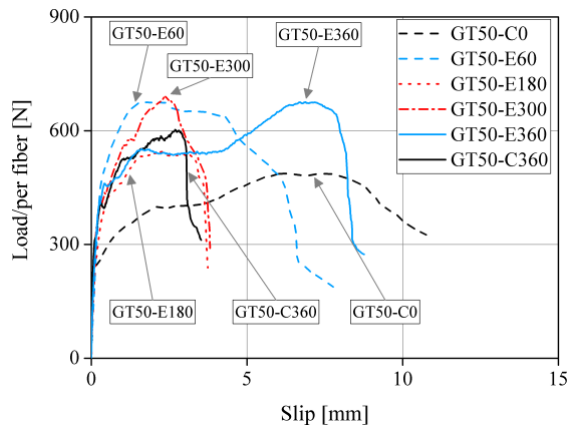
(b)



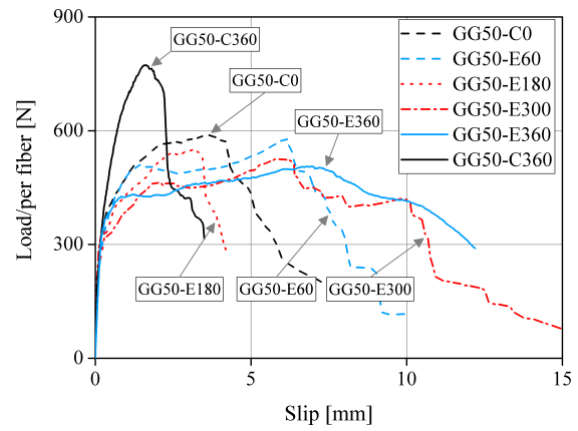
(c)

Fig. 12. Pull-out parameters of group steel-based TRM: (a) peak load; (b) debonding energy; (c) pull-out energy.

620



(a)



(b)

Fig. 13. Average of load-slip response of glass-based TRMs with different configurations: (a) GT50; (b) GG50.

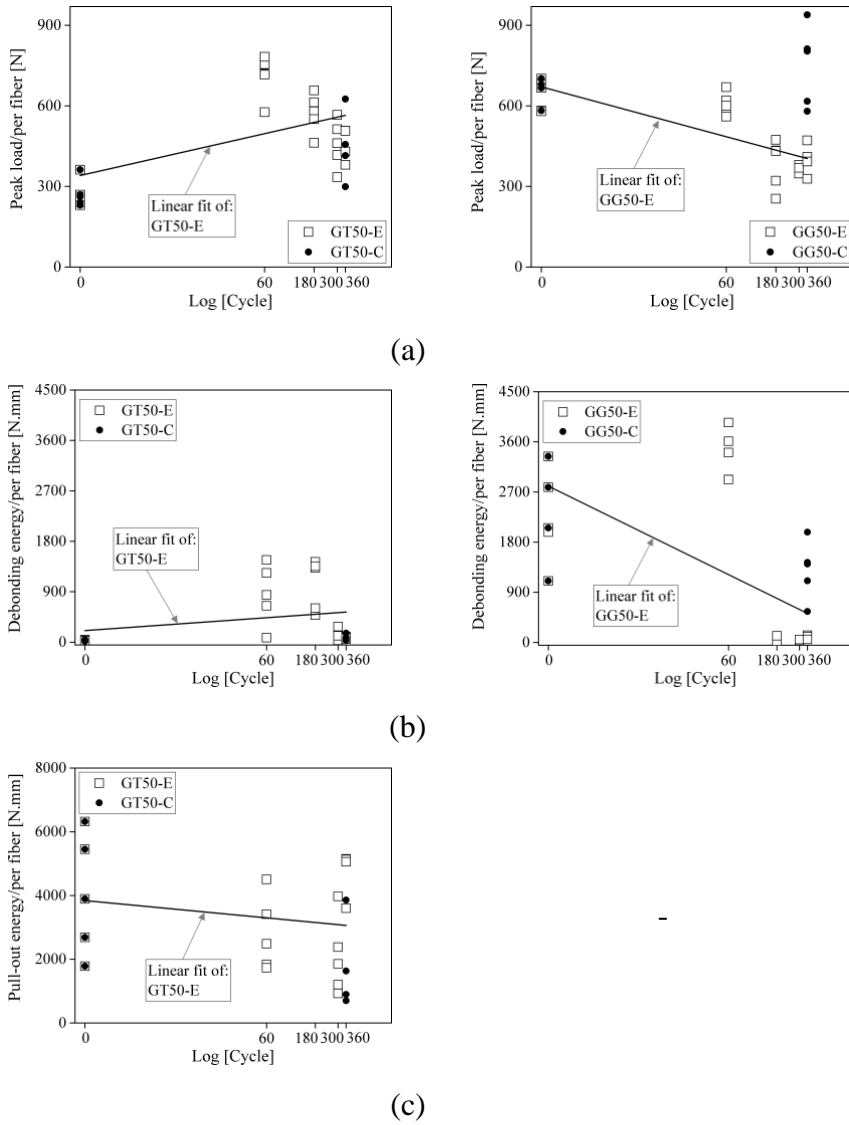


Fig. 14. Pull-out parameters of single+ transverse and group glass-based TRM: (a) peak load; (b) debonding energy; (c) pull-out energy.